JAM CM Journal of Applied Mathematics and Computational Mechanics 2025, 24(3), 31-45
www.amcm.pcz.pl p-ISSN 2299-9965
DOI: 10.17512/jamcm.2025.3.03 e-ISSN 2353-0588

ENHANCED STRENGTH OF SUBCRITICALLY PRELOADED PILLAR ARRAYS WITH REPLACEMENT OF FAILED ELEMENTS

Tomasz Derda

Department of Mathematics, Czestochowa University of Technology
Częstochowa, Poland
tomasz.derda@pcz.pl

Received: 4 May 2025; Accepted: 16 August 2025

Abstract. This paper presents the results of extensive numerical simulations using the fiber bundle model to investigate the effect of cyclic subcritical preloading of pillar arrays, in which failed elements are replaced after each loading cycle. The actual critical loading is applied after the cycling process. The preloading-replacement procedure alters the array's response from gradual failure under increasing load to abrupt failure. Consequently, after the cycling process, the onset of local failure inevitably triggers a global failure. Although the system's behavior becomes perfectly brittle, this approach allows for significant strengthening to be achieved in systems with at least moderate disorder.

MSC 2010: *82D30, 65C20, 82D80*
Keywords: *brittle behavior, cycling, fiber bundle model, preloading, strength enhancement*

1. Introduction

Failure in disordered materials is a complex phenomenon that attracts much attention in the communities of physicists, engineers, and material scientists [1, 2]. Fracture in disordered materials occurs through the initiation, growth, coalescence and propagation of micro-cracks, ultimately leading to macroscopic failure of the material [3]. At the nanometer scale, atomic displacement and defect motion can initiate irreversible deformation. While micro- and nanomaterials exhibit enhanced strength and toughness, they are also characterized by sample-to-sample fluctuations and non-trivial size effects [4]. Examples of materials at the micro/nanometer scale are arrays of micro/nanopillars, which can be considered as multi-component systems consisting of nearly identical elements. The applications and potential applications of micro/nanopillar arrays cover, for example, optical devices, sensors, energy generation devices, artificial retinas, cellular biomechanics, and tissue engineering [5, 6].

One of the statistical mechanical models of fracture is the fiber bundle model (FBM) [7]. In the classical version of this model, a set of fibers is subjected to a tensile load. The dynamics of the model is guided by the two parameters: amount of strength disorder of the system's elements and the range of stress redistribution after

an element's failure [8]. The interplay between quenched heterogeneites (in strength thresholds) and local stress concentrations that arise during the failure process is a complex phenomenon. Therefore, the systems show different failure modes, like nucleation, avalanche, or percolation. When the range of stress redistribution is very short, the failure process proceeds in the form of nucleation unless the amount of disorder is high. In this scenario, due to local stress concentration, we observe the growth of a single dominant cluster of broken fibers that consumes all other clusters. On the contrary, when the range of stress redistribution is high, the fracture process is in a percolation mode, local failures are uncorrelated and random in space [8-10]. These two behaviors are associated with two opposite and limiting load transfer rules, namely local load sharing (LLS) and global load sharing (GLS). Other intermediate load transfer rules have also been proposed and analyzed, such as the range-variable model [11, 12] or the R model [13-15].

Nucleation and percolation are two distinct failure modes that describe the internal propagation of damage within a system. These failure modes are often linked to the macroscopic response of the system, specifically the brittle and quasi-brittle phases [16-20]. In the case of purely brittle behavior, the global failure is triggered by the failure of the weakest element of the system. As a result, there is no stable state in this regime, and failure occurs abruptly. In the quasi-brittle scenario, by contrast, catastrophic collapse does not occur immediately. Failure of the entire system is preceded by a series of stable states at increasing load levels, and the system undergoes catastrophic collapse in an avalanche-like manner. A transition between brittle and quasi-brittle depends on the amount of strength disorder. As the amount of disorder is gradually increased, a transition occurs from the perfectly brittle phase to the quasi-brittle phase [16].

In this work, we apply the fiber bundle model approach to simulate arrays of (nano)pillars subjected to axial compression [21, 22]. In work [21], we have numerically studied the effect of optimally tailored cyclic preloading, assuming that pillar strength thresholds are not quenched. However, this study is a direct continuation of our previous study [23], where we analyzed the influence of eliminating a fraction of the system's elements before the actual critical loading. Here, we assume that the pillar strength thresholds are quenched, and a series of subcritical preloadings (each followed by the replacement of failed elements with new ones) is applied until the brittle phase is reached. The effect of substitution was previously studied in work [24], where a small portion of fibers of one type had been replaced by another type of fibers that were stronger than the original ones. In turn, in [25], the authors analyze failure processes in systems consisting of two types of fibers: breakable and unbreakable. Instead, we adopt a different approach in this study: elements that fail during subcritical preloading are replaced with nearly identical ones, whose strength thresholds are drawn from the same probability distribution as those of the original pillars in the system.

2. Arrays of pillars under two-stage loading

The system under consideration is composed of $N = L \times L$ almost identical pillars, which are geometrically arranged at the nodes of a square grid and subjected to axial loading. Under load, each pillar can be in one of two states: intact or crushed. Failure of the pillar occurs when the applied load exceeds its strength threshold σ_{th}^{i}, $i = 1, 2, \ldots, N$. Indeed, the distribution of pillar strength thresholds is the only parameter that controls the disorder in the system. Therefore, the strength threshold is the sole difference between system components. In this work, we employ two types of distributions to randomly generate pillar strength thresholds: the uniform distribution (on the interval [0, 1]) and the Weibull distribution. The cumulative distribution function of the latter is given by

$$P(\sigma_{th}) = 1 - \exp\left[-\left(\frac{\sigma_{th}}{\lambda}\right)^{\rho}\right] \tag{1}$$

where ρ and λ are shape and scale parameters, respectively. The parameter ρ (also known as the Weibull index) governs the amount of disorder in the system – the higher the value of the parameter, the lower the disorder of the pillar strength thresholds. The scale parameter is set to $\lambda = 1$. The Weibull distribution has a much stronger physical foundation than the uniform distribution and is commonly employed to model the stochastic failure characteristics of components in fracture phenomena, spanning length scales from the nanometer scale to that of earthquakes, by adjusting the Weibull index [26].

The loading procedure is carried out in a quasi-static manner. The complete realisation of this process is performed as follows. The initial external load, F, is set to 0. Then, the external load is uniformly increased on all intact pillars by an amount δF, sufficient to cause the failure of a single pillar. After the failure of the pillar, the increase of external load is stopped, and the load is redistributed from the failed pillar to the intact ones, according to a given load transfer rule. The load transfer may provoke the next failures and is repeated until a stable state is reached, i.e., when the load transfer no longer causes further failures. Then, the external load is uniformly increased again by an amount sufficient to destroy a single intact pillar. This process continues until the complete failure of the system under the critical load F_c. The number of pillars destroyed between two consecutive load increments is called an avalanche (Δ). The total number of avalanches during the entire process can be seen as the failure time of the system, t_f. The load F_c is associated with the ultimate strength of the system, and the avalanche triggered by F_c is referred to as the catastrophic avalanche.

The range of load transfer can be modeled using an appropriate load transfer rule. The shortest possible range of load transfer is represented by the LLS rule. In this scheme, only the nearest surviving neighbors of the crushed pillar take on an additional load. The rule that neglects the distance between the crushed pillar and the intact ones is the GLS rule. In this case, the load from the failed pillar is equally

transferred to all intact pillars in the system, regardless of their distance from the broken element – all pillars in the system are considered equidistant in the mathematical sense. Hence, this rule constitutes a mean-field approximation. The rule that interpolates between the extreme cases is the so-called range variable (RV) rule. The load $\Delta q_{i\to j}$ allocated to the j-th intact pillar is expressed as:

$$\Delta q_{i\to j} = \frac{Z_i}{|r_j - r_i|^\gamma}\Delta Q_i \tag{2}$$

where ΔQ_i is the load of the failed i-th pillar, $|r_j - r_i|$ is the distance between the j-th intact pillar and the i-th crushed one, γ is a parameter, and Z_i is a normalization factor that guarantees the load conservation. By tuning γ, we can transition from the GLS rule ($\gamma = 0$) to LLS rule ($\gamma \to \infty$).

Our simulation-based experiment is divided into two stages. The first stage involves cyclic subcritical preloading followed by the replacement of crushed components with intact ones after each cycle. Hence, each preloading-replacement cycle results in a structural repair of the array. The strength thresholds of the newly inserted pillars follow the same distribution as the thresholds of the initial components. Each cycle ends at the time step $t_f - 1$, just before the occurrence of the catastrophic avalanche, and lasts up to the load F_{sub}, which directly precedes the critical load F_c. Therefore, F_{sub} is the last load for which the system remains in a pre-critical state. The number of cycles (η) is a random variable, as cycling ends when $F_{sub} = 0$, i.e., at the cycle where the system becomes so unstable that the failure of a single component (microscopic failure) inevitably results in a self-sustaining catastrophic avalanche, causing total system collapse (macroscopic failure). Let $t_f(i)$ denote the failure time of the system after i-th cycle, where $i = 0, 1, \ldots, \eta$ (with $i = 0$ referring to no preloading). The failure time is defined as the number of avalanches occurring during the entire critical loading process. We observe $N \geq t_f(0) \geq t_f(\eta) = 1$, which means that the system transitions from quasi-brittle behavior to perfectly brittle behavior as a result of the cyclic preloading-replacement process. The equality $t_f(0) = t_f(\eta)$ holds only in the case when the initial system is already purely brittle. On the other hand, equality $t_f(0) = N$ occurs exclusively if the array undergoes complete destruction through a sequence of single-element avalanches. It is noted that, due to the quasi-static nature of the loading process, we consider only values of F that trigger successive avalanches, with $F = 0$ being the initial load. Consequently, $F_{sub} = 0$ after the η-th cycle, as previously mentioned.

The second stage focuses on the critical loading of the system that has previously undergone the cycling process described above. It is noted that at the beginning of the critical loading, all nodes in the grid are occupied by intact components. However, due to the replacements made during the first stage of the experiment, the distribution of pillar strength thresholds differs from the initial one. To compare arrays of different sizes, the critical load is scaled by the system size as $\sigma_c = F_c/N$. In practice, we have performed simulations of critical loading for each system after every

preloading-replacement cycle, including the case without any preloading cycles. This allows us to obtain a sequence $\sigma_c(0), \sigma_c(1), \ldots, \sigma_c(\eta)$ where $\sigma_c(i)$ denotes the critical load after i-th preloading-replacement cycle, with $i = 0, 1, \ldots, \eta$. The final value in the sequence, $\sigma_c(\eta)$, corresponds to the ultimate load-bearing capacity of the system after all cycles have been completed. Accordingly, the ratio $\varphi = \sigma_c(\eta)/\sigma_c(0)$ serves as a measure of the system's strengthening induced by the full sequence of preloading-replacement cycles.

3. Simulation results and discussion

Based on the model described in the previous section, we have implemented a Python code to simulate two-stage loading processes in the pillar arrays. First, for each analyzed system size, we generated and stored $M = 10^4$ configurations of initial threshold sets, denoted as $\left\{\sigma_{th}^i(0)\right\}_{i=1}^N$, where each set contains N threshold values assigned to the array's elements. We conducted simulations across a broad range of system sizes, ranging from $N = 40 \times 40$ to $N = 500 \times 500$ for the LLS rule, and $N = 1000 \times 1000$ for the GLS rule. In the case of the RV rule, due to its higher computational cost, we restricted the simulations to two system sizes, namely $N = 60 \times 60$ and $N = 100 \times 100$. To gain a detailed understanding of the effect of the load transfer range, we have varied the value of γ from 0 (pure GLS) to 10, which is close to the behavior of the LLS rule. To investigate the influence of disorder in pillar strength thresholds, we have examined a uniform distribution on the interval [0,1], as well as a Weibull distribution with $\rho = 2, 3, 4, \ldots, 10, 12$. This allows us to explore a range of disorder levels, from relatively higher disorder (uniform distribution, $\rho = 2$) to relatively lower disorder ($\rho = 10$, $\rho = 12$). Averages were calculated over M samples.

Before analyzing the actual simulation results, a natural question arises: which components are destroyed during the preloading phase? In systems with long-range interactions (GLS-like behavior), the damage pattern is spatially random (percolation-like), meaning that primarily the weakest components fail. In contrast, in systems governed by short-range interactions (LLS-like behavior), damage tends to localize into clusters. In such cases, the failure of a component is influenced not only by its intrinsic strength but also by its spatial location within the array. Consequently, failure affects not only the weakest elements but also some stronger ones that are located in locally weak regions.

After each preloading cycle, the crushed components (typically the weakest ones) are replaced with new ones, whose strength thresholds are sampled from the same distribution as those of the initial components. This iterative preloading-replacement process inevitably leads to an enhancement of the system's load-bearing capacity, such that $\sigma_c(0) < \sigma_c(1) < \ldots < \sigma_c(\eta)$. Thus, by completing the cycling process, we can determine the upper limit of σ_c for an array whose initial pillar strength thresholds are sampled from a given distribution and which is subsequently subjected to a cyclic preloading-replacement procedure that transforms the system's

response from quasi-brittle to perfectly brittle behavior. It should be noted that $\sigma_c(\eta) = \min\left(\{\sigma_{th}^i(\eta)\}_{i=1}^N\right)$.

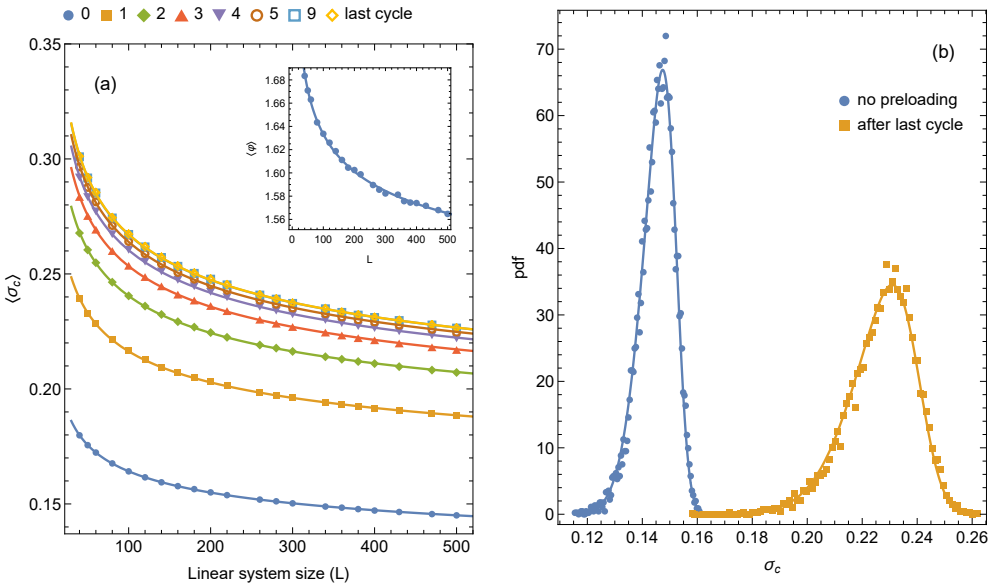

Fig. 1. (a) Mean critical load $\langle\sigma_c\rangle$ after i-th cycle (see legend) as a function of the linear system size L. Data points correspond to LLS systems with initially uniformly distributed strength thresholds. Solid lines are drawn according to equation (3), with parameters computed from the samples. The inset shows the mean strengthening of these LLS systems after completing the full cycling process. (b) Empirical distribution of σ_c for LLS systems with $N = 500 \times 500$ and an initially uniform distribution of strength thresholds. The solid lines represent a skew-normal distribution fitted to the data

Figure 1a shows the empirical mean critical loads for LLS systems with initially uniform strength thresholds. The data presented in the figure refers to the mean critical loads after the i-th cycle, as well as the results after the complete preloading-replacement procedure. It is seen that the effect of each subsequent preloading--replacement cycle is weaker than that of the previous one. This indicates that the most significant strengthening occurs during the initial cycles, after which the system continues to gain strength with each subsequent cycle, albeit at a diminishing rate, eventually approaching a state of perfectly brittle behavior. Qualitatively similar behavior is observed for the GLS systems. The known [23, 26, 27] two-parameter formula for the LLS mean critical load (average failure strength), given by:

$$\langle\sigma_c^{\mathrm{LLS}}(N)\rangle = \frac{\alpha}{(\ln\sqrt{N})^{\beta}} \tag{3}$$

also holds for our LLS systems after each cycle (α and β are fitting parameters). Moreover, this provides the appropriate formula for the mean strengthening $\langle\varphi\rangle$, as shown by the solid line in the inset of Figure 1a. The size effect on the critical load, characteristic of LLS systems, becomes more pronounced after the complete

preloading-replacement procedure, as reflected in the shape of the $\langle\varphi\rangle$ curve. As the system goes through subsequent cycles, the variability of critical loads also changes – the standard deviation is noticeably greater for systems after complete cycling compared to those with no cycling (see Fig. 1b). Effectively, the post-cycling distribution reflects the distribution of the weakest strength thresholds across individual systems.

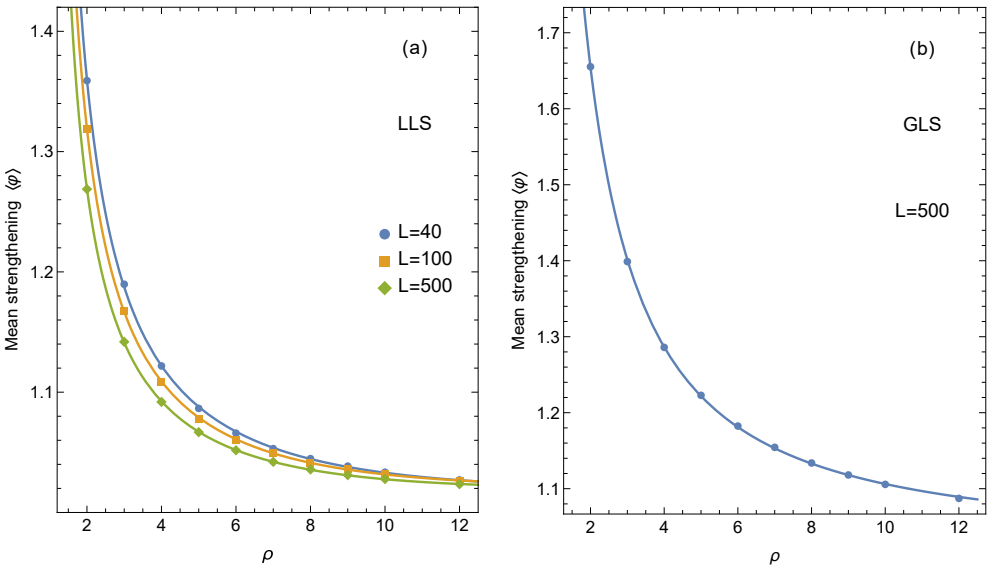

Fig. 2. Mean strengthening of LLS (a) and GLS systems (b) as a function of ρ. Data points represent simulation results, while solid lines show fits based on formula (4) for LLS and formula (5) for GLS, with parameters obtained from data fitting

The effect of disorder on the strengthening of the system is graphically reported in Figure 2. It is seen that $\langle\varphi\rangle$ is a decreasing function of ρ for both the GLS and LLS rules. Thus, as the system disorder decreases, the strengthening ratio also decreases, reaching a value of 1 in the case of a homogeneous system (a system without disorder). The dependence on system disorder is also evident in the size effect related to the strengthening of LLS systems (see Fig. 2a). A pronounced size effect is observed in the case of relatively high disorder ($\rho = 2$). However, as the parameter ρ increases, the size effect gradually weakens, becoming almost negligible for relatively homogeneous (low-disorder) systems ($\rho = 12$). In contrast, in GLS systems, the size effect is already weak at low values of ρ (present primarily due to statistical fluctuations) and becomes virtually absent in the low-disorder regime. Therefore, for clarity, Figure 2b shows data corresponding to a single system size, namely $L = 500$.

For both extreme load transfer rules, we propose formulas for the mean strengthening as a function of ρ, assuming a fixed system size. In the case of LLS systems, a good approximation is provided by

$$\langle\varphi_N^{\mathrm{LLS}}(\rho)\rangle = \frac{a_1 \cdot \rho^{b_1}}{(\ln\rho)^{c_1}} \tag{4}$$

whereas function suitable for the GLS systems can be expressed as

$$\langle \varphi_N^{\mathrm{GLS}}(\rho)\rangle = a_2 + \frac{b_2}{\rho^{c_2}} \tag{5}$$

where $a_1, b_1, c_1, a_2, b_2, c_2$ are fitting parameters.

The mean macroscopic strength of the GLS systems without preloading is known from the literature [7, 26, 28-30]. The mean critical load, $\langle \sigma_c^{\mathrm{GLS,pre}}(N)\rangle$, decreases with increasing system size N, and in the thermodynamic limit it converges to a finite, non-zero value – in contrast to the behavior observed in LLS systems. For uniformly disordered systems, the asymptotic (macroscopic) strength is given by $\sigma_c^{\mathrm{GLS}}(\infty) = = 0.25$. The mean critical load for finite systems can be approximated by the following formula

$$\langle \sigma_c^{\mathrm{GLS}}(N)\rangle = 0.25\left(1 + 1.2656N^{-2/3}\right). \tag{6}$$

Initially uniformly distributed GLS systems, transformed by the complete preloading-replacement process, are described by the expression

$$\langle \sigma_c^{\mathrm{GLS,post}}(N)\rangle = 0.5\left(1 + 0.4385N^{-0.3565}\right), \tag{7}$$

which gives $\sigma_c^{\mathrm{GLS,post}}(\infty) = 0.5$, and as a result, $\varphi_{N\to\infty}^{\mathrm{GLS}} = 2$. For finite-size systems, we have obtained $\langle \varphi^{\mathrm{GLS}}(N)\rangle = 2\left(1 + 0.2196N^{-0.3043}\right)$. Therefore, the strengthening ratio for the GLS systems is greater than for the LLS systems (see inset in Fig. 1a).

The critical load for Weibull-distributed GLS systems tends to $(\rho e)^{-1/\rho}$ as the system size N goes to infinity. The approximating formula for finite-size systems is as follows:

$$\langle \sigma_c^{\mathrm{GLS}}(\rho, N)\rangle = (\rho e)^{-1/\rho}\left(1 + 0.996N^{-2/3}\left(\frac{e^{2/\rho}}{\rho}\right)^{1/3}\right). \tag{8}$$

We have found that, after the complete preloading-replacement process, the mean critical load can be fitted by the following three-parameter expression:

$$\langle \sigma_c^{\mathrm{GLS,post}}(\rho, N)\rangle = (\rho e)^{-1/\rho}\cdot a_3 \cdot \left(1 + b_3 \cdot N^{-c_3}\right) \tag{9}$$

where a_3, b_3, c_3 are parameters that depend on ρ. Based on the fitting results, the parameters take value in the ranges $b_3 \in (0.106, 0.433)$ and $c_3 \in (0.363, 0.451)$. The parameters b_3 and c_3 account for the finite-size correction, while the most significant parameter in the formula (9) is a_3, which controls the strengthening of the system. Interestingly, we observe that $\langle \varphi_N^{\mathrm{GLS}}(\rho)\rangle \gtrapprox a_3(\rho)$, becoming nearly equal for larger system sizes. This observation supports the conjecture that the asymptotic limit satisfies $\varphi_{N\to\infty}^{\mathrm{GLS}}(\rho) = a_3(\rho)$. The results of the fittings using Eqs. (8) and (9) are illustrated in Figure 3, along with the inset showing the fitted values of the parameter a_3 as a function of ρ.

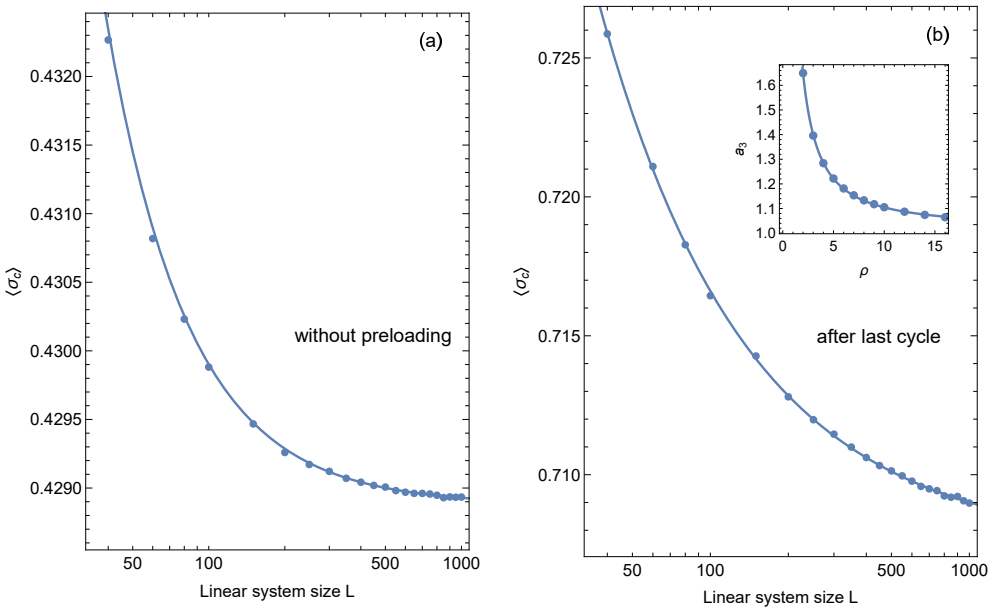

Fig. 3. Mean critical load for GLS systems with initially Weibull-distributed pillar strengths ($\rho = 2$), evaluated under two scenarios: (a) without the preloading-replacement process, and (b) after the complete cycling process. The empirical data shown in the left panel are fitted using Eq. (8), while the right panel data are approximated by Eq. (9). The inset displays the fitted values of the parameter a_3 from Eq. (9) modeled by the function given in Eq. (5) with corresponding parameters

As previously noted, the strengthening ratio is higher in GLS systems compared to their LLS counterparts. This applies to both cases studied: systems with initially uniform strength distributions and those with initially Weibull-distributed thresholds (see Fig. 2). This behavior is associated with another important measure of the system's overall robustness: the fraction d of failed elements that the system can tolerate before a catastrophic avalanche leads to the collapse of the entire system. We assume that each preloading cycle stops just before the onset of the catastrophic avalanche. Consequently, $d_c(i) = N_c(i)/N$ represents the critical fraction of crushed elements during the i-th preloading cycle ($i = 1, 2, \ldots, \eta$), where N_c denotes the total number of the failed pillars within this i-th cycle. It follows that $N_c(\eta) = 0$. Thus, after each cycle, N_c pillars are replaced with new ones, and the resulting preloading-replacement-transformed distribution of pillar strength thresholds increasingly deviates from the initial one as the fraction of elements replaced during cycling increases.

Figure 4 shows the mean critical fraction, $\langle d_c \rangle$, of failed elements during successive steps of the cycling process. For both analyzed rules, the critical fraction is a rapidly decreasing function of the cycle number. Thus, in terms of strengthening, the initial steps of the preloading-replacement process are crucial, as they involve the highest fraction of failed pillars, which are subsequently replaced with new ones. We observe that $\langle d_c^{\mathrm{LLS}} \rangle \ll \langle d_c^{\mathrm{GLS}} \rangle$ (see inset in Fig. 4). The no-cycled LLS systems can tolerate only a relatively small amount of damage, d, before the collapse of the

system, compared to their GLS counterparts. Therefore, since the fraction of replaced pillars is smaller in the case of the LLS scheme, the strengthening of LLS systems is also less pronounced. However, when analyzing the effectiveness of the preloading--replacement process as the ratio between the achieved mean strengthening (which can be regarded as the *gain*) and the mean total fraction, $\langle \sum_{i=1}^{\eta} d_c(i) \rangle$, of replaced pillars during the entire cycling process (interpreted as the *cost* or *price*), the LLS scheme proves to be more efficient (see Table 1). The LLS cycling enables the effective removal of weak regions at relatively low cost ($\langle \varphi^{\mathrm{LLS}} \rangle - 1 > \langle \sum_{i=1}^{\eta} d_c^{\mathrm{LLS}}(i) \rangle$), whereas in the GLS systems, the relation $\langle \varphi^{\mathrm{GLS}} \rangle - 1 \approx \langle \sum_{i=1}^{\eta} d_c^{\mathrm{GLS}}(i) \rangle$ holds. Especially, for relatively low-disorder LLS systems, we observe $\langle \varphi^{\mathrm{LLS}} \rangle - 1 \gg \langle \sum_{i=1}^{\eta} d_c^{\mathrm{LLS}}(i) \rangle$ – that is, the achieved mean strengthening is around 3-4%, attained by replacing noticeably less than 1% of N. Finally, it should be noted that some elements located at specific nodes can be replaced multiple times during the cycling process.

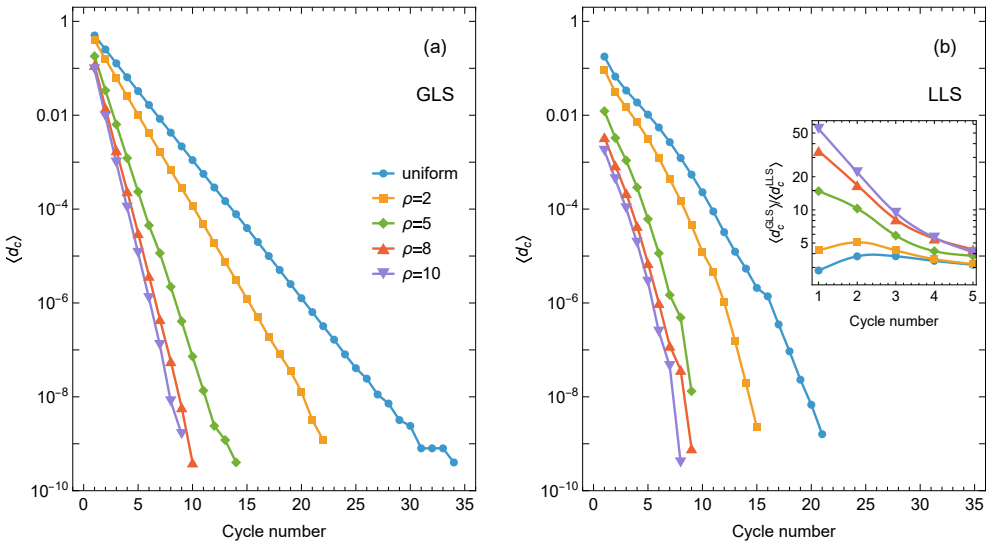

Fig. 4. Mean critical fraction of failed pillars, $\langle d_c \rangle$, during the i-th preloading step as a function of cycle number for (a) GLS systems and (b) LLS systems. The inset presents the relation $\langle d_c^{\mathrm{GLS}} \rangle / \langle d_c^{\mathrm{LLS}} \rangle$ over the first five cycles. System size $N = 500 \times 500$

In the final part of this section, we analyze the effect of interaction range by applying the RV rule. Figure 5a shows the mean critical loads after a selected number of preloading-replacement cycles, as well as after the complete cycling process. As γ increases, the effective range of interactions decreases, shifting the system from long-range interactions ($\gamma = 0$, where all elements are equidistant) to short-range interactions that closely resemble those in the pure LLS scheme ($\gamma = 10$). However, in con-

trast to the pre-cycling $\langle\sigma_c^{\mathrm{RV,pre}}(\rho)\rangle$, the post-cycling function $\langle\sigma_c^{\mathrm{RV,post}}(\rho)\rangle$ is non-monotonic. Initially, as the system slightly departs from the pure GLS scheme, an increase in the post-cycling mean critical load is observed up to $\gamma\approx 1.7$. It is known that the crossover from the mean-field limit to short-range interactions occurs near $\gamma_c = 2$ [11]. Therefore, the post-cycling mean critical load is an increasing function of γ through nearly the entire range of the mean-field regime and begins to decrease just before the crossover to the regime of short-range interactions. By examining the mean strengthening as a function of γ, this behavior is evident for all analyzed initial system disorders (Fig. 5b). The strengthening is most pronounced for $\gamma\in(1.4,1.7)$ (approximately). Apparently, there seems to be a tendency for the maximum of the strengthening to shift gently towards higher values with increasing system size and towards lower values as the initial disorder decreases.

Table 1. Comparison of the mean total fraction of replaced pillars and the system strengthening resulting from the complete cycling process in GLS and LLS systems. System size $N = 500\times 500$

Initial system disorder	GLS		LLS	
	$\langle\sum_{i=1}^{\eta} d_c^{\mathrm{GLS}}(i)\rangle$	$\langle\varphi^{\mathrm{GLS}}\rangle$	$\langle\sum_{i=1}^{\eta} d_c^{\mathrm{LLS}}(i)\rangle$	$\langle\varphi^{\mathrm{LLS}}\rangle$
uniform	1.0102	2.0092	0.3173	1.5647
$\rho=2$	0.6555	1.6553	0.1497	1.2688
$\rho=3$	0.3990	1.3989	0.0599	1.1419
$\rho=4$	0.2860	1.2860	0.0300	1.0919
$\rho=5$	0.2229	1.2228	0.0170	1.0668
$\rho=6$	0.1825	1.1825	0.0104	1.0517
$\rho=7$	0.1544	1.1544	0.0067	1.0421
$\rho=8$	0.1338	1.1338	0.0045	1.0357
$\rho=9$	0.1181	1.1181	0.0032	1.0310
$\rho=10$	0.1057	1.1057	0.0023	1.0278

We noted earlier that for both the LLS and GLS rules, the initial cycles are crucial, while later cycles are almost negligible – a pattern that also holds for $\gamma\approx 0$ and $\gamma\gtrsim 3$. This is not the case for γ around 1.7 (see Fig. 5a). However, the shape of the curve $\langle\sigma_c^{\mathrm{RV}}(\rho)\rangle$ after the initial two cycles closely resembles that of systems without a preloading-replacement process. Yet after the third cycle, the shape of the curve starts to deviate from that of $\langle\sigma_c^{\mathrm{RV,pre}}(\rho)\rangle$. Compared to the pure GLS scheme ($\gamma\approx 0$) or long-range interactions, the effect of the later steps of the cycling process decays more slowly around $\gamma = 1.7$. This is accompanied by a considerably greater average number of cycles relative to the case of $\gamma = 0$ (see Fig. 6a). The fastest cycling process is for the LLS-like systems. These LLS-like systems are also associated with the greatest fraction of original pillars that remain intact after the complete cycling process (see Fig. 6b). The mean fraction of remaining intact original elements is highly negatively correlated with the obtained strengthening.

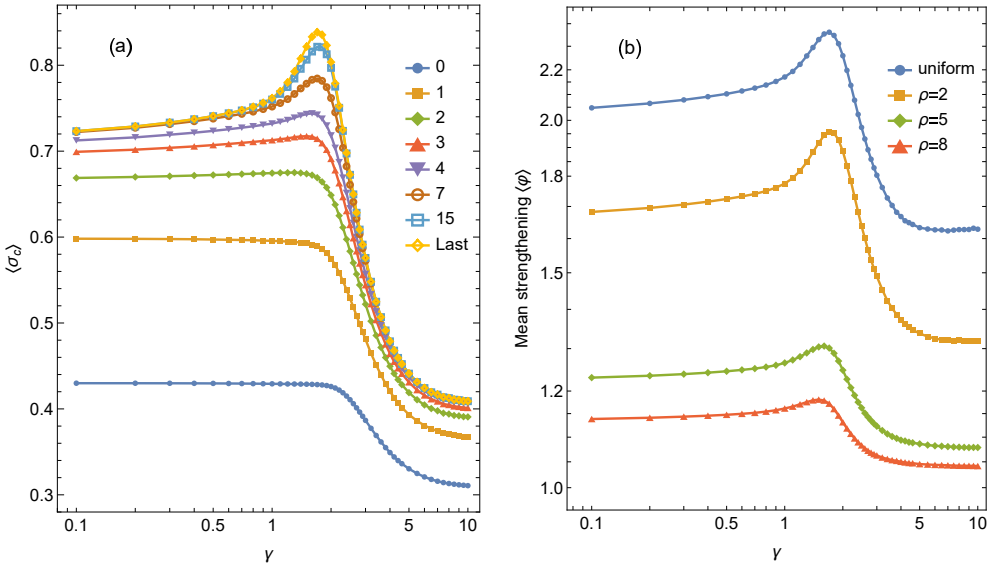

Fig. 5. (a) Mean critical loads after the i-th cycle (see legend) as a function of the parameter γ. Systems of size $N = 100 \times 100$ with initially Weibull-distributed pillar strength thresholds ($\rho = 2$). (b) Mean strengthening, $\langle \varphi^{\mathrm{RVM}} \rangle$, as a function of the parameter γ. Systems of size $N = 100 \times 100$

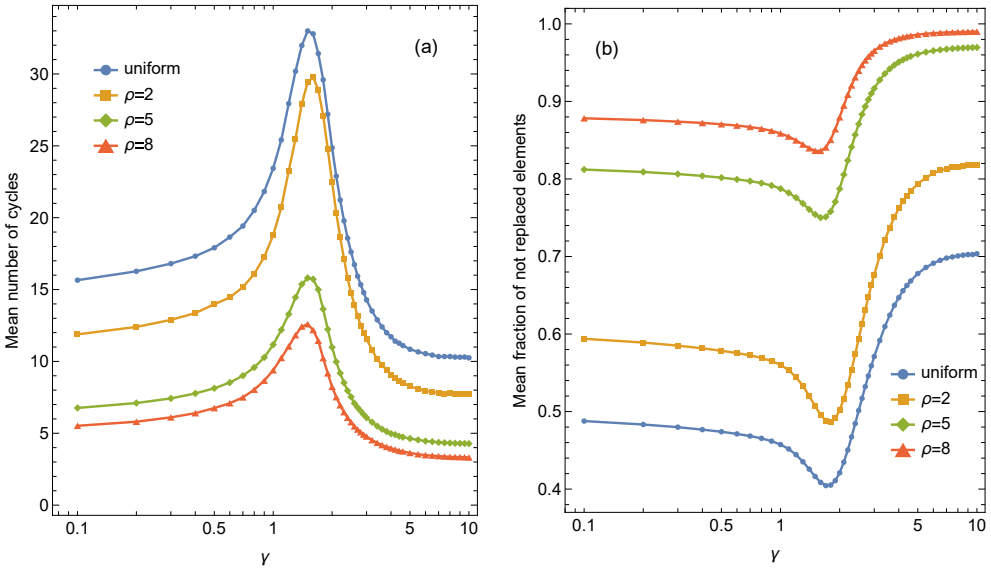

Fig. 6. (a) Mean number of preloading-replacement cycles as a function of γ. (b) Mean fraction of initial elements that survive the cycling process as a function of the parameter γ. Systems of size $N = 100 \times 100$

The reason why the mean strengthening at $\gamma \approx 1.7$ is more efficient than in the limiting case of $\gamma = 0$ can be explained as follows. As the parameter γ increases, the effective range of interactions decreases – there is an interplay between global and local load redistribution. At $\gamma \approx 1.7$ the load transfer becomes sufficiently localized

to effectively eliminate elements from the weakest regions during preloading, while still maintaining the character of mean-field regime to prevent the early triggering of a catastrophic avalanche. Thus, $\gamma \approx 1.7$ provides an optimal level of an effective range of interactions.

In the work [23], we simulated the critical loading of arrays under the RV rule, previously subjected to subcritical preloading without the replacement of the failed elements. The results of those simulations differ qualitatively from those produced by the cyclic preloading-replacement procedure. Under the pure GLS scenario ($\gamma = 0$), we observed virtually no effect of subcritical preloading on the critical load. A strengthening effect became evident in the regime of short-range interactions, increasing in magnitude as the effective interaction range decreased. However, during the transition from a regime dominated by long-range interactions to one dominated by short-range interactions, a weakening was observed, with a peak around $\gamma \in (1.7, 2)$. In contrast, in this range of γ, the influence of cyclic preloading combined with the replacement of failed elements is particularly noticeable, as it is accompanied by a strengthening greater than in the GLS-like and LLS-like cases, with the most pronounced strengthening occurring near $\gamma = 1.7$.

4. Conclusions

We have conducted computer simulations of critical loading in arrays of pillars, which were previously subjected to cyclic subcritical preloading together with the replacement of failed elements. As a result, the preloading-replacement-transformed distributions of pillar strength thresholds deviate from those observed in the non-preloaded systems, with particularly significant differences in relatively highly disordered systems. The systems are effectively purged of their weakest elements.

The applied cycling stops after the cycle in which the number of replaced pillars is zero. This ensures that the resulting systems display perfectly brittle behavior: catastrophic collapse occurs abruptly after the failure of a single element, and the systems cannot tolerate any pre-critical damage. However, since the disorder in the strength of the system's elements plays a key role in the failure process, the post-cycling systems exhibit an increase in macroscopic strength compared to non-preloaded systems. The scale of strengthening depends on the applied load transfer rule, the size of the system, and the initial disorder of the system. The strengthening ratio is an increasing function of the amount of disorder in the system. By analyzing two extreme load transfer rules – namely, the GLS and LLS rules – we observed a stronger strengthening effect in the mean-field regime. Nevertheless, the strengthening process is more efficient in the LLS case, as a noticeable increase in strength is achieved through the insertion, during the cycling process, of a relatively small number of new pillars.

The rule that interpolates between the global load sharing and local load sharing schemes is the range variable rule. By varying the value of γ between 0 and 10, one can transition from pure GLS to LLS-like systems. Computer simulations revealed

that, unlike in non-preloaded systems, the post-cycling mean critical load is not a monotonically decreasing function of γ. Instead, throughout most of the mean-field regime, it increases, with the strengthening effect being most pronounced for $\gamma \in (1.4, 1.7)$. Beyond this range, both the post-cycling mean critical load and the mean strengthening begin to decrease.

References

[1] Chakrabarti, B.K., & Benguigui, L.G. (1997). *Statistical Physics of Fracture and Breakdown in Disordered Systems*. Oxford University Press.

[2] Herrmann, H.J., & Roux, S. (1990). *Statistical Models for the Fracture of Disordered Media*. Amsterdam: North-Holland.

[3] Roy, S. (2016). Interplay of stress release range and disorder in fracture, PhD thesis. The Institute of Mathematical Sciences, Chennai.

[4] Taloni, A., Vodret, M., Costantini, G., & Zapperi, S. (2018). Size effects on the fracture of microscale and nanoscale materials. *Nat. Rev. Mater.*, *3*, 211-224.

[5] Park, J.E., Won, S., Cho, W., Kim, J.G., Jhang, S., Lee, J.G., & Wie, J.J. (2021). Fabrication and applications of stimuli-responsive micro/nanopillar arrays. *J. Pol. Sci.*, *59*, 1491.

[6] He, X., Jin, L., Qin, Y., Zhong, J., Ouayang, Z., & Zeng, Y. (2024). Advances in micropillar arrays in cellular biomechanics detection and tissue engineering. *Biocell*, *48*(11), 1521-1529.

[7] Hansen, A., Hemmer, P.C., & Pradhan, S. (2015) *The Fiber Bundle Model: Modeling Failure in Materials*. Wiley-VCH.

[8] Roy, S. (2021). From nucleation to percolation: The effect of system size when disorder and stress localization compete. *Front. Phys.*, *9*, 752086.

[9] Biswas, S., Roy, S., & Ray, P. (2015). Nucleation versus percolation: Scaling criterion for failure in disordered solids. *Phys. Rev. E*, *91*, 050105.

[10] Ray, P. (2018). Statistical physics perspective of fracture in brittle and quasi-brittle materials. *Phil. Trans. R. Soc. A*, *377*, 20170396.

[11] Hidalgo, R.C., Moreno, J., Kun, F., & Herrmann, H.J. (2002). Fracture model with variable range of interaction. *Phys. Rev. E*, *65*, 046148.

[12] Biswas, S., & Goehring, L. (2016). Interface propagation in fiber bundles: Local, mean-field and intermediate range-dependent statistics. *New J. Phys.*, *18*, 103048.

[13] Roy, S., Biswas, S., & Ray, P. (2017). Modes of failure in disordered solids. *Phys. Rev. E*, *96*, 063003.

[14] Roy, S., Biswas, S., & Ray, P. (2019). Failure time in heterogeneous systems. *Phys. Rev. Res.*, *1*, 033047.

[15] Derda, T. (2022). Suddenly loaded arrays of pillars with variable range of load transfer. *JAMCM*, *21*(4), 16-27.

[16] Danku, Z., Pál, G., & Kun, F. (2023). Size scaling of failure strength at high disorder. *Physica A: Stat. Mech. Appl.*, *624*, 128994.

[17] Kádár, V., Pál, G., & Kun, F. (2020). Record statistics of bursts signals the onset of acceleration towards failure. *Sci. Rep.*, *10*, 2508.

[18] Kun, F., Allan, L., Batool, A., Danku, Z., & Pál, G. (2024). Failure process of fiber bundles with random misalignment. *Phys. Rev. Res.*, *6*, 033344.

[19] Roy, S., & Goswami, S. (2018). Fiber bundle model under heterogeneous loading. *J. Stat. Phys.*, *170*, 1197-1214.

[20] Kádár, V., Danku, Z., & Kun, F. (2017). Size scaling of failure strength with fat-tailed disorder in a fiber bundle model. *Phys. Rev. E*, *96*, 033001.

[21] Derda, T., & Domanski, Z. (2020). Enhanced strength of cyclically preloaded arrays of pillars. *Acta Mech.*, *231*, 3145-3155.

[22] Derda, T., & Domanski, Z. (2021). Survivability of suddenly loaded arrays of micropillars. *Materials*, *14*(23), 7173.

[23] Derda, T. (2023). Critical loading of pillar arrays having previously eliminated elements. *JAMCM*, *22*(4), 18-29.

[24] Sbiaai, H., Hader, A., Boufass, S. et al. (2019). The effect of the substitution on the failure process in heterogeneous materials: Fiber bundle model study. *Eur. Phys. J. Plus*, *134*, 148.

[25] Kovács, K., Hidalgo, R.C., Pagonabarraga, I., & Kun, F. (2013). Brittle-to-ductile transition in a fiber bundle with strong heterogeneity. *Phys. Rev. E*, *87*, 042816.

[26] Pál, G., Danku, Z., Batool, A., Kádár, V., Yoshioka, N., Ito, N., Ódor, G., & Kun, F. (2023). Scaling laws of failure dynamics on complex networks. *Sci. Rep.*, *13*, 19733.

[27] Pradhan, S., Hansen, A., & Chakrabarti, B.K. (2010). Failure processes in elastic fiber bundles. *Rev. Mod. Phys.*, *82*, 499.

[28] McCartney, L.N., & Smith, R.L. (1983). Statistical theory of the strength of fiber bundles. *J. Appl. Mech.*, *50*(3), 601-608.

[29] Smith, R.L. (1982). The asymptotic distribution of the strength of a series-parallel system with equal load-sharing. *Ann. Probab.*, *10*(1), 137-171.

[30] Porwal, P.K., Beyerlein, I.J., & Phoenix, S.L. (2006). Statistical strength of a twisted fiber bundle: an extension of Daniels equal-load-sharing parallel bundle theory. *JoMMS*, *1*(8), 1425-1447.